Nano Research

ISSN 1998-0124 CN 11-5974/O4
https://doi.org/10.1007/s12274-023-6396-1

Research Article

Polydopamine-coated photoautotrophic bacteria for improving extracellular electron transfer in living photovoltaics

Melania Reggente[1] (✉), Charlotte Roullier[1], Mohammed Mouhib[1], Patricia Brandl[1], Hanxuan Wang[1], Stefano Tacconi[2], Francesco Mura[3], Luciana Dini[2], Rossella Labarile[4], Massimo Trotta[4], Fabian Fischer[5,6], and Ardemis A. Boghossian[1] (✉)

[1] *Institute of Chemical Sciences and Engineering (ISIC), Ecole Polytechnique Fédérale de Lausanne (EPFL), Lausanne 1015, Switzerland*
[2] *Department of Biology and Biotechnology Charles Darwin, Sapienza University of Rome, Rome 00185, Italy*
[3] *Research Center on Nanotechnology Applied for Engineering of Sapienza (CNIS), University of Rome Sapienza, Rome 00185, Italy*
[4] *CNR-IPCF Consiglio Nazionale delle Ricerche – Istituto per i Processi Chimico Fisici, Bari 70126, Italy*
[5] *Institute of Life Technologies, HES-SO Valais-Wallis, Sion 1950, Switzerland*
[6] *Institute for Renewable Energy, HES-SO Valais-Wallis, Sion 1950, Switzerland*

Received: 19 June 2023 / **Revised:** 3 November 2023 / **Accepted:** 4 November 2023

ABSTRACT

Living photovoltaics are microbial electrochemical devices that use whole cell–electrode interactions to convert solar energy to electricity. The bottleneck in these technologies is the limited electron transfer between the microbe and the electrode surface. This study focuses on enhancing this transfer by engineering a polydopamine (PDA) coating on the outer membrane of the photosynthetic microbe *Synechocystis* sp. PCC6803. This coating provides a conductive nanoparticle shell to increase electrode adhesion and improve microbial charge extraction. A combination of scanning electron microscopy (SEM), transmission electron microscopy (TEM), UV–Vis absorption, and Raman spectroscopy measurements were used to characterize the nanoparticle shell under various synthesis conditions. The cell viability and activity were further assessed through oxygen evolution, growth curve, and confocal fluorescence microscopy measurements. The results show sustained cell growth and detectable PDA surface coverage under slightly alkaline conditions (pH 7.5) and at low initial dopamine (DA) concentrations (1 mM). The exoelectrogenicity of the cells prepared under these conditions was also characterized through cyclic voltammetry (CV) and chronoamperometry (CA). The measurements show a three-fold enhancement in the photocurrent at an applied bias of 0.3 V (vs. Ag/AgCl [3 M KCl]) compared to non-coated cells. This study thus lays the framework for engineering the next generation of living photovoltaics with improved performances using biosynthetic electrodes.

KEYWORDS

biophotovoltaics, bioelectronics, photosynthetic bacteria, cyanobacteria, polydopamine, adherence

1 Introduction

Biophotovoltaics (BPVs) are electrochemical devices that rely on biological/electrode interactions to convert solar energy to electricity. Whole-cell devices can use self-replicating photoautotrophic microbes, such as cyanobacteria, to harness sunlight and transfer electrons across their outer membranes. These microbes can perform these functions while actively sequestering CO_2 for biomass production. During this process, the sunlight is absorbed by microbial light-harvesting pigments [1–3] that activate a water-splitting reaction in the reaction centers of the thylakoid membranes. The resulting charge separation triggers a cascade of intracellular redox reactions in the photosynthetic electron transport chain, leading to the formation of the essential metabolites nicotinamide adenine dinucleotide phosphate (NADPH) and adenosine triphosphate (ATP) [4–6]. Under intense light exposure, excess electrons can be exported extracellularly and transferred to anodes that act as terminal electron acceptors through a mechanism called exoelectrogenicity [4–10]. The resulting extracellular electron transfer (EET) can occur via either direct contact between the electrode and outer membrane redox proteins, such as cytochromes, or mediators that will carry electrons from the cell to the anode surface [2, 5, 11]. Because of the lack of effective EET pathways in cyanobacteria, these devices show relatively low power efficiencies [3, 5]. Although calculations by McCormick et al. [1] predict current densities in the range of 0.34 to 2.46 mA/cm^2, the highest values reported thus far remain on the order of 0.06 mA/cm^2 [12].

Several strategies have been developed to improve the performances of these devices, such as optimizing the electrode material and geometry [13–23] and biochemically modifying the microbes [24–29]. The former approach improves EET by optimizing the microbe-electrode interaction. Several studies have shown that the electronic exchange between the microbe and the electrode can be enhanced using conductive polymers [21, 23]. These studies show a decrease in the electrode surface impedance with 3D-structured electrodes made of porous indium tin oxide (ITO) [15] or pillared structures [22] that can increase cell loading.

Address correspondence to Melania Reggente, melania.reggente@epfl.ch; Ardemis A. Boghossian, ardemis.boghossian@epfl.ch

The latter approach for improving device performance includes bioengineering microbes to synthesize specific mediators [24] or electron-shuttling cytochromes [25–27] as well as embedding membrane-bound conductive nanomaterials [28, 29]. These approaches, which aim to improve the charge extraction, can be used with techniques that can promote cell viability. Such techniques include the encapsulation of microbes with artificial conductive coatings [30–35, 38–43]. For example, living yeast cells have been coated with silica [31] and calcium carbonate [32] to provide the microbe with an additional protection layer against harsh environments. A similar approach has been applied to *Chlorella* sp. green algae that have been encapsulated in a titanium oxide shell [33].

Several studies have explored the application of soft polymers as long-lasting functional coatings for living cells. Among these polymers, polypyrrole (PPy) and polydopamine (PDA) have been polymerized *in situ* on the surface of several microbes. These polymers have been found to enhance the bioelectrochemical properties of fungal strains like *Aspergillus niger* [34] and natural exoelectrogens like *Shewanella oneidensis* MR-1 [35, 43] as well as purple nonsulfur bacteria like *Rhodobacter capsulatus* [44]. The PDA in particular benefits from biocompatible adhesive properties that show low toxicity. This bioinspired synthetic polymer is produced through the self-polymerization of dopamine (DA) [36–38] under mild conditions [41]. When used to encapsulate individual yeast cells, the PDA was shown to increase the resistance of the cells to environmental stress without interfering with the cell division and metabolism. The coating even enabled further functionalization of the microbe with other functional molecules [39, 40]. Since the PDA consists of several redox-active quinone and catechol groups, it can be used to further boost EET during extracellular respiration, as demonstrated in several microbial fuel cell applications [42, 43]. Previous studies have also demonstrated the *in situ* polymerization of PDA on the surface of *Streptomyces xiamenensis* and *Rhodotorula glutinis* cells. In these studies, the PDA behaves as a redox mediator for improving catalytic activity [42] and enhancing electron transfer at the biological/inorganic interface [43].

Despite its promises as a biocompatible and exoelectrogenic coating, PDA has largely remained unexplored for photoautotrophic applications. This work therefore investigates the chemical polymerization of DA directly onto the outer membrane of the cyanobacterium *Synechocystis* sp. PCC 6803. This work further examines the PDA effects on the microbe's viability and exoelectrogenicity.

2 Experimental

2.1 Microbial cell culture

Wildtype *Synechocystis* sp. PCC 6803 precultures were prepared by adding 10 mL 1× BG11 medium [45] to a 100 mL Erlenmeyer flask. The flask was inoculated with healthy cells from a BG11-agar plate and left to grow for 16 to 24 h at 30 °C and 180 rpm under continuous illumination (50 μE, white light). When the optical density at 750 nm ($OD_{750\ nm}$) of the cell suspension reached a value between 2.5 and 5, cell precultures were diluted in 250 mL Erlenmeyer flasks with fresh 1× BG11 to obtain 20 mL cell cultures with a starting $OD_{750\ nm}$ of 0.2. The cell cultures were left to grow for 2 days before harvesting them in their mid-exponential growth phase ($OD_{750\ nm}$ ~ 2–2.5).

2.2 PDA-coated *Synechocystis*

To chemically coat *Synechocystis* sp. PCC 6803 with PDA, the cells were grown to their mid-exponential phase. These cells were then harvested and diluted in 50 mL Eppendorf tubes to achieve an $OD_{750\ nm}$ = 2 in 5 mL of solution. Cell suspensions were successively washed and resuspended in 10 mM phosphate buffer (PB) supplemented with 10 mM NaCl and 5 mM $MgCl_2$. The final pH was adjusted either to 7.5 or to 8.2 with 1 M NaOH. Finally, three different concentrations (1, 5 and 15 mM) of dopamine hydrochloride (DA, Sigma Aldrich) were added to the cell suspension and incubated for 3.5 h at 30 °C and 180 rpm under continuous illumination (50 μE, white light). For the control measurements, the DA solutions were prepared in the absence of cyanobacteria cells following the same procedure described above. Untreated wildtype *Synechocystis* cells were also incubated in PB for 3.5 h prior to performing the electrochemical measurements. The formation of PDA was confirmed by absorbance measurements in the 200–900 nm range (Shimadzu 3600 Plus UV–Vis–NIR Spectrophotometer). The spectra were recorded directly after the addition of DA (t = 0 h) and prior to the harvesting (t = 3.5 h).

2.3 Morphological and structural characterization of PDA-coated *Synechocystis*

Scanning and transmission electron microscopies (SEM and TEM, respectively) were used to assess the formation of PDA on the cell. Unmodified *Synechocystis* and PDA-coated cells were fixed with 2% paraformaldehyde and 0.2% glutaraldehyde in 0.1 M cacodylate buffer (pH 7.2) for 2 h. For the SEM analysis, the cells were deposited on a polylysine-coated glass coverslip and postfixed with 1% OsO_4 in the same buffer for 1 h on ice. After washing with 0.1 M cacodylate buffer (pH 7.2), the cells were dehydrated with ethanol (EtOH) at increasing concentrations (50%, 75%, 95% and 100%). This step was followed by chemical drying with 1:1 EtOH and hexamethyldisilazane (HMDS, Sigma-Aldrich) for 20 min, incubation in pure HMDS for 1 h, and finally, overnight drying and evaporation. The specimens were then mounted on aluminum stubs and imaged using a Zeiss Merlin microscope (Zeiss, Oberkochen, Germany). To increase the electron conductivity, some of the specimens were also coated with a 3-nm thick layer of chromium using a quorum Q150 T sputter (Quorum Technologies, UK) and imaged using a Zeiss Auriga SEM (Zeiss).

For the TEM analysis, the fixed samples were stained with 0.5% uranyl acetate overnight at 4 °C. The samples were then dehydrated with ethanol (30%, 50%, 70%, and 100%) and embedded in Spurr resin. Thin sections of 60 nm were cut with an ultramicrotome (Powertome PC, RMC Boeckeler Instruments) and placed on 200-mesh copper grids. The TEM measurements were performed using a Zeiss Auriga SEM (Zeiss) equipped with an STEM module operating at 20 keV.

The confocal Raman spectroscopy measurements were performed using an inVia Raman Microscope (Renishaw). The spectra were recorded at an excitation wavelength of 532 nm (1% laser power) in the 600–2200 cm^{-1} range using a 100× objective and a diffraction grating of 1800 cm^{-1}.

2.4 Oxygen evolution experiments

The cells were harvested during their mid-exponential growth phase by centrifugation and resuspended in 1 mL of freshly prepared 1× BG11 medium to an $OD_{750\ nm}$ of 2 or 1 (for higher light exposure). The oxygen concentration under light and dark conditions for whole cells was monitored at room temperature using a Clark-type electrode (Hansatech, OxyLab+). Samples were illuminated at an intensity of 200 μmol photons/(m^2·s) under white light. To provide the cells with an excess carbon source, 10 mM of sodium bicarbonate ($NaHCO_3$) was added to the cell suspensions in the reaction chamber before the oxygen

measurements were taken. The oxygen production rates were normalized using the total chlorophyll a (Chl a) content. Chl a extraction was performed by pelleting and disrupting the cells by centrifugation at 15,000 rpm at 4 °C for 10 min. After discarding the supernatant, the pellets were resuspended in 1 mL 4 °C methanol and incubated in the dark for a minimum of 2 h. One last centrifugation was conducted at 15,000 rpm and 4 °C, and the green supernatant was separated from the blue pellet to measure its absorbance at 665 and 720 nm against a methanol blank. The Chl a content was calculated using the equation (Eq. (1)) [46]:

$$\text{Content}_{(\text{Chl a})}\ (\mu\text{g/mL}) = 12.9447 \times (A_{665\ \text{nm}} - A_{720\ \text{nm}}) \quad (1)$$

2.5 Visible and fluorescence imaging

Cells were fixed onto polylysine-coated glass-bottom petri dishes by spotting 30 µL of the cell suspension at $OD_{750\ nm}$ ~ 2 for 30 min followed by washing with PB. The cells were then covered with 50 µL of freshly prepared PB (pH 7.4). For the confocal imaging, the cells were imaged using a custom-built optical setup consisting of an inverted microscope (Eclipse Ti-E, Nikon AG Instruments) with an oil-immersion total internal reflection fluorescence (TIRF) 100× objective (numerical aperture 1.49, Nikon) coupled to a CREST X-Light spinning-disk confocal imaging system (CREST Optics) (60 µm pinholes) and an InGaAs camera (NIRvana 640 ST, Princeton Instruments) with a 0.4 µm step-size, as previously described [47, 28]. Samples were illuminated using a TriLine LaserBank system (Cairn Research) at 640 nm, and the cells' autofluorescence was imaged with an 800 nm (Chroma) long-pass filter (Semrock) to remove contributions from the excitation source. Visible images were acquired using an EMCCD camera (iXonUltra 888, Andor) under the illumination of a halogen lamp.

2.6 Bioanode preparation

Graphite rods (3.05 mm diameter, Thermo Scientific) were cut into 2-cm long electrodes. They were sonicated for 10 min in deionized water before sonication in 70 vol.% EtOH. Cells grown to their mid-exponential phase were harvested and diluted in 50 mL Eppendorf tubes to achieve an $OD_{750\ nm}$ = 2 in 5 mL of PB solution. Samples were pelleted, and the supernatant was removed after centrifugation at 4000 rpm for 15 min at room temperature. The pellets were washed once with 5 mL PB solution. The pellets were then gently resuspended in 100 µL PB. A 20 µL aliquot of this cell suspension was casted onto a graphite rod electrode and left to settle at room temperature until a humid, flat pellet was obtained. To avoid cell detachment during the electrochemical measurements, the cells were encased in a dialysis cellulose membrane (14 kDa molecular weight pore size, Sigma Aldrich) that was incubated in PB for 30 min and fixed with a Teflon cap (Starlab) and parafilm [21, 23, 26]. For the control involving the physical mixture of PDA and unmodified *Synechocystis* cells, a PDA pellet was resuspended in 100 µL PB. 20 µL of this solution was then directly added to an unmodified *Synechocystis* pellet.

2.7 Electrochemical characterization

Measurements were taken in a three-electrode electrochemical cell using the graphite-based bioanodes as the working electrode. A Pt wire was used as the counter electrode and a standard Ag/AgCl (3M KCl) electrode as the reference. The system was connected to a MultiPalmsens4 potentiostat (Palmsens BV) equipped with the Multitrace 4.4 software. PB (pH 7.4) was used as the electrolyte under unmediated conditions. The PB was supplemented with 1 mM $K_3Fe(CN)_6$ (Sigma Aldrich) for experiments performed under mediated conditions. Light exposure was provided by a white LED lamp with an intensity of 370 µE. Cyclic voltammograms (CV) in the −0.1 – +0.4 V range were collected at a scan rate of 5 mV/s prior to performing the potentiostatic measurements. The system was left to equilibrate by conducting chronoamperometry (CA) measurements that were taken over 17 h under unmediated conditions at a constant applied potential of 300 mV (vs Ag/AgCl). The $K_3Fe(CN)_6$ was then added to the solution to a final concentration of 1 mM, and the CA measurements were taken during the light-dark cycles (1 h each).

2.8 Cell adherence test

SEM imaging was used to compare the adherence of coated cells to 1-cm diameter graphite foil-based electrodes (0.254 mm thick, Thermoscientific). Briefly, 100 µL aliquots of the cell suspensions at an optical density OD_{750} = 10 in 1× BG11 were deposited onto the electrodes and incubated for 15 h in the dark at 30 °C. Following incubation, 80 µL of the supernatant was removed, and samples were washed twice with 100 µL deionized water before being left to air dry. The cells were then fixed with 2% paraformaldehyde and 0.2% glutaraldehyde in 0.1 M cacodylate buffer (pH 7.2) for 3 h and dehydrated with dimethylformamide (DMF) at increasing concentrations (25%, 50%, 75%, and 90% in deionized water). Samples were imaged using a Zeiss Merlin microscope with an Everhart-Thornley detector. Triplicate samples were prepared and imaged for both coated and uncoated cells.

3 Results and discussion

The PDA was synthesized from different concentrations of DA that had been added to *Synechocystis* sp. PCC 6803 cells that were collected during mid-exponential growth. Previous studies have shown the polymerization to occur under alkaline conditions [48], initiated by the oxidation of DA by dissolved oxygen (O_2) [49]. The DA-cell suspension was therefore incubated under slightly alkaline conditions for 3.5 h until the color of the cell suspension became darker. The SEM images taken at the conclusion of the reaction show a rougher surface morphology for the PDA-coated cells compared to the unmodified cells (Fig. 1(a)). In particular, the SEM shows the formation of small globules on the surface of the cells, indicative of PDA nanoparticle formation. The coverage and packing of these nanoparticles are shown to vary with pH, with denser packing observed at a higher pH of 8.2 compared to the cells prepared at a lower pH of 7.5. At both pH values, the images also show a concentration-dependent packing. The nanoparticles show denser surface coverage at a higher DA concentration of 5 mM compared to 1 mM, though the concentration dependence is more readily discernable at the lower pH of 7.5 where the surface coverage is further from saturation. Even higher DA concentrations of 15 mM led to increased precipitation of PDA aggregates and to poor cell encapsulation (Fig. S1 in the Electronic Supplementary Material (ESM)), leaving several parts of the outer membrane uncovered. These results confirm the concentration- and pH-dependent formation of PDA, with maximum surface coverage achieved at moderate concentrations.

The localization of these nanoparticles was also confirmed by TEM (Fig. 1(b)). The TEM images show the nanoparticles to largely localize along the periphery of the cells. These observations are consistent with the increased globular surface morphology of the cells that was observed in the SEM images of Fig. 1(a). The nanoparticles appear sub-100 nm in size, which is also consistent with the sizes in the SEM images. The TEM images, however, show limited nanoparticle formation in the interior of the cells. These results indicate the PDA polymerization to be largely limited to the exterior of the *Synechocystis* cells under the tested conditions.

The polymerization of the PDA was also confirmed by absorption and Raman spectroscopies (Fig. 2). Absorbance spectra

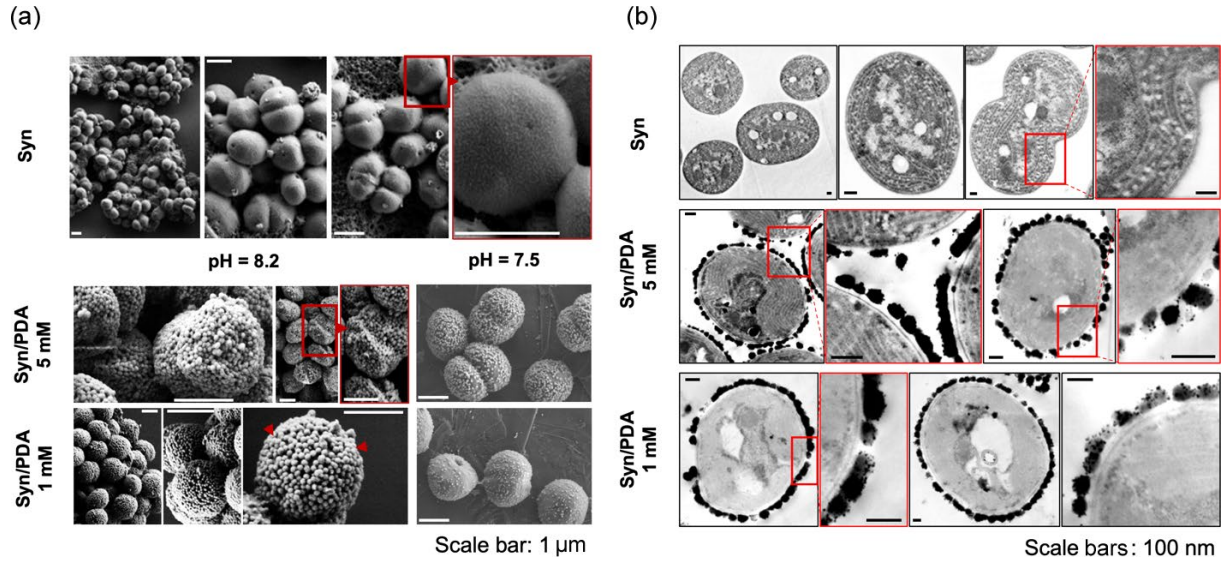

Figure 1 Surface encapsulation of *Synechocystis* cells by PDA. (a) SEM micrographs of unmodified *Synechocystis* (top) and of PDA-coated cells obtained through the oxygenic polymerization of 5 mM (middle) and 1 mM (bottom) DA. PDA formation was performed at pH 8.2 (left) and pH 7.5 (right). Red arrows point to individual PDA nanoparticles on the cell surface. (b) TEM micrographs of unmodified *Synechocystis* (top) and of PDA-coated cells obtained through the oxygenic polymerization of 5 mM (middle) and 1 mM (bottom) DA dissolved in a PB solution at pH 8.2. Red squares highlight areas with corresponding higher resolution images shown on the right.

were taken immediately after the addition of the DA (t = 0 h) and after the reaction completion (t = 3.5 h) (Fig. 2(a)). The spectra of control cells (green) and PDA-coated cells (gray) are similar except for the peak centered at 280 nm. This peak corresponds to absorption from the DA monomers, which also appear in the control measurements of PDA in the absence of the cells (blue). The absorption peak at 426 nm, on the other hand, corresponds to the absorption of the PDA. This peak, shown in the inset, increases during the polymerization from t = 0 h to t = 3.5 h, confirming the formation of PDA. Despite the ca. 5-fold increase in absorption, the peak intensity remained quite small ($A_{426\ nm}$ = 0.025 at t = 3.5 h) as relatively low DA concentrations were used for these measurements. The limited absorption of the PDA at these concentrations can be used to concomitantly monitor the absorption peaks of the cells within this range. As shown in the spectra, both the spectra of untreated *Synechocystis* (green) and PDA-treated (gray) cells show three characteristic absorption peaks assigned to the Chl a at 436 nm, the photosynthetic systems at 680 nm, and the phycocyanin (PC) pigments at 625 nm [52]. These peaks are observed even at the end of the reaction (t = 3.5 h) on polymerization of the PDA. These measurements thus confirm light absorption by the photosynthetic pigments of the cell even in the presence of PDA under the tested conditions.

Raman spectroscopy was also used to chemically confirm the formation of PDA (Fig. 2(b)). The spectrum of wildtype *Synechocystis* cells (green) exhibits three peaks centered around 1005, 1156 and 1519 cm^{-1} corresponding to the vibrational and rocking modes of cellular carotenoid molecules. The 1005 cm^{-1} peak arises from the coupling of the plane rocking modes of the methyl groups attached to the polyene backbone and that of the C–C bonds, while the peak at 1519 cm^{-1} represents the stretching vibrations of C=C double bonds in the polyene chain of the carotenoid. The peak at 1156 cm^{-1} represents the second vibrational mode of the C-C single bond [50]. Moreover, the spectrum of the PDA aggregates (blue) synthesized without the microbes shows three bands at 1590, 1401, and 1340 cm^{-1}. These bands correspond to the aromatic rings of the polymer [51]. The spectra of PDA-coated cells contain the peaks from both the PDA without the cells and the *Synechocystis* cells without the PDA. The relative intensities of the PDA peaks are shown to increase with increasing DA addition (Fig. S2 in the ESM) while retaining the features of the photosynthetic pigments from the cells.

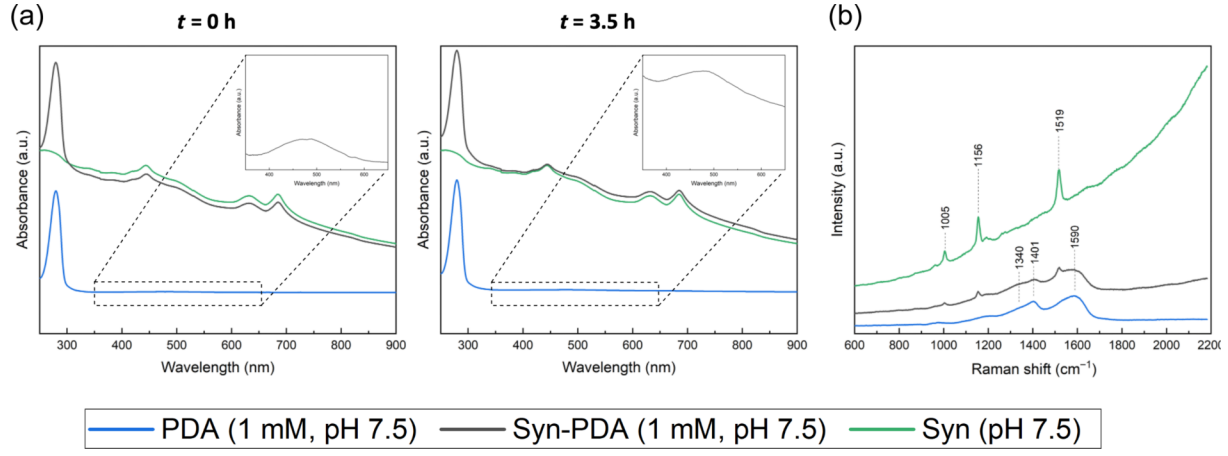

Figure 2 Chemical characterization of PDA formation on *Synechocystis* cells. (a) UV–Vis absorption spectra of unmodified *Synechocystis* (Syn, green), *Synechocystis* cells incubated in 1 mM DA in PB at pH 7.5 (Syn-PDA, gray), and 1 mM DA in PB in the absence of cells at pH 7.5 (PDA, blue). Spectra were acquired immediately after the addition of DA (t = 0 h, left) and at the end of the reaction (t = 3.5 h, right). (b) Raman spectra of PDA (blue), unmodified *Synechocystis* cells (green), and PDA-coated cells (gray). Measurements were taken at 532 nm excitation.

The effect of the PDA on cell viability was examined with oxygen evolution and growth experiments (Fig. 3). As shown in Fig. 3(a), the PDA treatment contributes to a decrease in the oxygen evolution rates compared to the untreated control cells. Oxygen evolution is shown to decrease both with increasing DA concentration and increasing pH, conditions that favor PDA formation. At high PDA concentrations that show the greatest decrease in oxygen evolution, we further observe cell clustering (Fig. S3(a) in the ESM). These clusters may contribute to inter-cell light shielding, diminishing the photosynthetic activity and oxygen evolution. Consequently, *Synechocystis* cells that show the least PDA surface coverage and cluster formation (1 mM DA at pH 7.5) also show the smallest diminution in photosynthetic activity. Under these synthesis conditions, the cells were able to recover their oxygen evolution rates relative to the untreated cells by increasing light exposure with lower cell densities and higher light intensities (Fig. 3(b)). Furthermore, the PDA-treated cells under these synthesis conditions show a growth rate that is comparable to that of untreated cells over the course of seven days (Fig. 3(c)). Cell growth was monitored by recording absorbance at 750 nm, where light absorption by the PDA and cell pigments is minimal. Though previous studies have reported diminished cell growth in the presence of internalized nanoparticles [28], these effects were overcome with increased illumination, compensating for the competitive light absorption of the nanoparticles. In this case, the PDA nanoparticles are shown to largely localize outside the cell, and the sustained cell growth suggests that the PDA does not impede cell division. Furthermore, the competitive light absorption should diminish as the PDA to biomass ratio decreases with cell growth over time. These observations are consistent with the sustained autofluorescence (Fig. 3(d) and Fig. S3(b) in the ESM) of the treated cells, which reflects cell viability. Given the recovery and preservation of the cell viability, these PDA synthesis conditions (1 mM DA, pH 7.5) were used for further study.

The exolectrogenicity of the cells was studied using a three-electrode system with a graphite rod as the working electrode. The PDA-coated cells, uncoated *Synechocystis* cells, and abiotic PDA control were drop-casted onto graphite electrodes, left to settle for approximately 30 min, encased in a cellulose membrane, and immersed in PB solution. CV measurements of the PDA-coated cells taken at the start of the experiment showed a peak at 0.23 V corresponding to DA oxidation (Fig. 4(a)). The peak was shown to decrease over each successive CV cycle, reflecting a progressive decrease in the concentration of oxidizable species, in this case DA, as reported previously [54]. These observations are consistent with measurements taken for the biotic control in the absence of PDA, as the uncoated cells showed no intial redox peak and no significant change in capacitance (Fig. S4 in the ESM). To stabilize the electrode prior to mediated CA measurements, current was collected while under a constantly applied potential of 0.30 V (vs. Ag/AgCl) under cyclic 1-h light/1-h dark conditions used in previous studies (Fig. S5(a) in the ESM) [13–23]. After 17 h, the PDA-coated cells show stabilized photocurrent, overlapping with the photoresponse of the abiotic PDA electrodes. This residual photocurrent is attibuted to the PDA photoactivity, which shows a concentration- and pH-dependent response similar to that of other photoactive polymer coatings (Fig. S6 in the ESM) [23]. The stabilization of the electrode was confirmed by CV measurements,

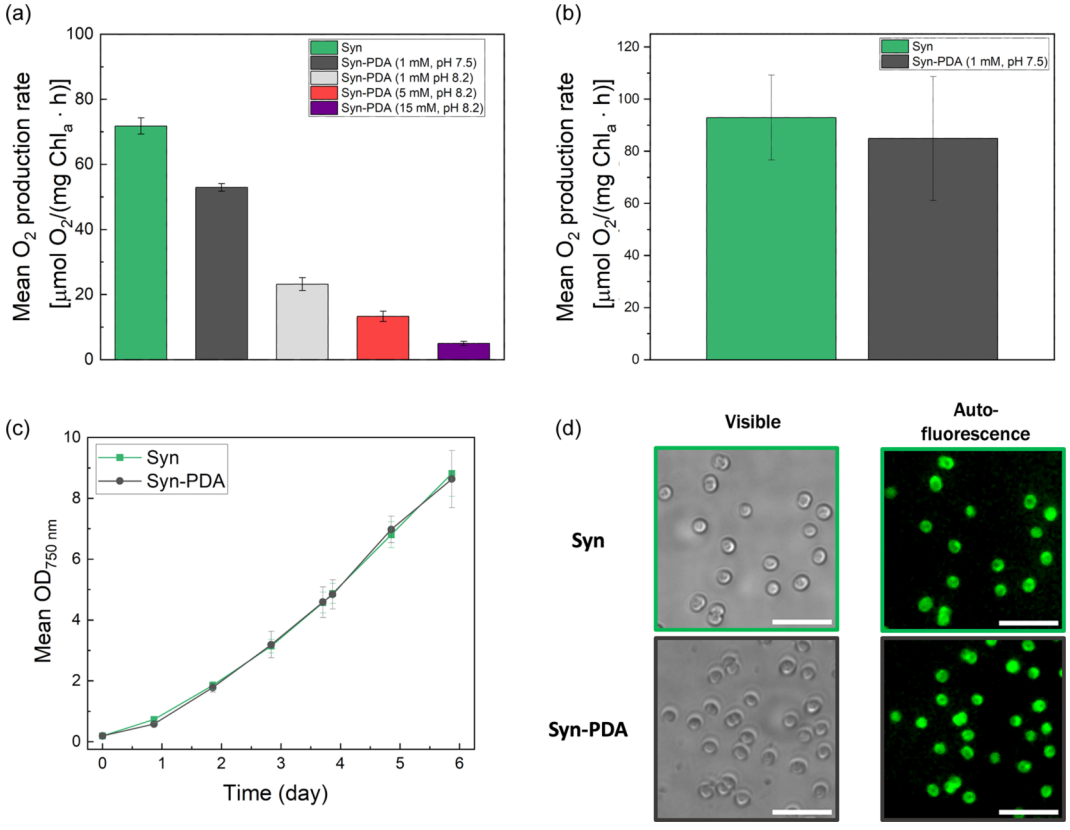

Figure 3 Effect of PDA encapsulation on cell activity and viability. (a) Net oxygen production rate of illuminated untreated *Synechocystis* cells and PDA-coated cells prepared in the presence of various DA concentrations at pH 7.5 and pH 8.2. Measurements were normalized by the Chl a content and are based on three independent experiments. Error bars represent one standard deviation. (b) Net oxygen production rate of illuminated untreated *Synechocystis* cells (Syn, green) and PDA-coated cells (PDA-Syn, gray) prepared in the presence of 1 mM DA at pH 7.5. Measurements were recorded at an optical density at 750 nm ($OD_{750\ nm}$) of 1 and normalized by the Chl a content. Error bars represent one standard deviation. (c) Growth curves of three biological triplicates of *Synechocystis* (green) and PDA-coated *Synechocystis* (gray) cells based on optical density measurements at 750 nm ($OD_{750\ nm}$). The PDA-coated cells were prepared in the presence of 1 mM DA at pH 7.5. (d) Representative visible (left) and confocal fluorescence (right) images of unmodified *Synechocystis* cells (top) and cells incubated with 1 mM DA at pH 7.5 (bottom). Measurements were taken at an excitation of 640 nm with emissions collected above 800 nm. Scale bar: 10 μm. Additional images can be found in Fig. S3 in the ESM.

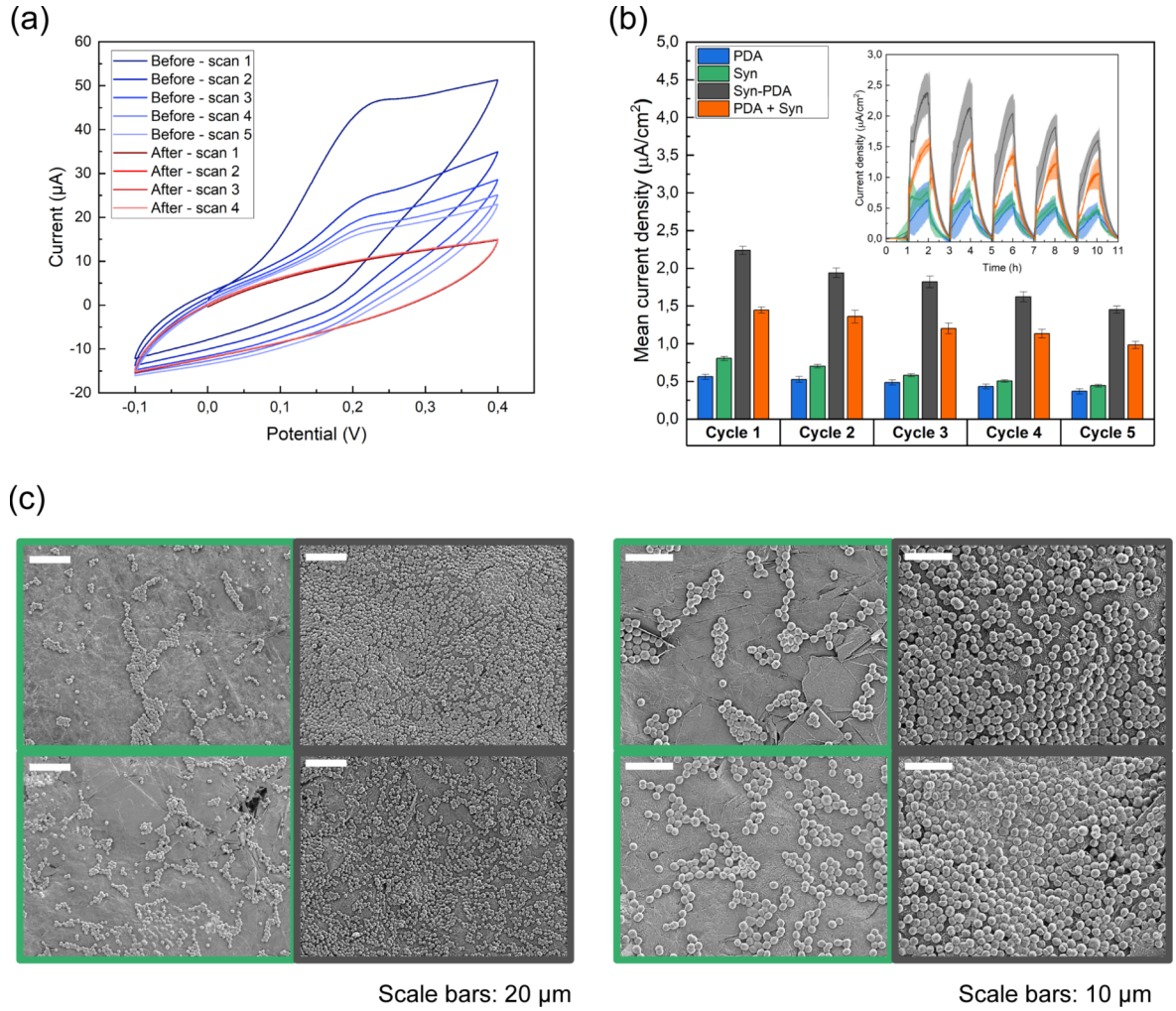

Figure 4 Electrogenic activity of PDA-coated *Synechocystis* cells. (a) CVs of PDA-coated *Synechocystis* cells that were incubated in 1 mM DA at pH 7.5. Measurements were taken at a scan rate of 5 mV/s with a graphite working electrode before ("blue") and after ("red") stabilization following unmediated CA measurements at an applied potential of 0.3 V (vs. Ag/AgCl) for 17 h under cyclic light-dark conditions. (b) Histogram representing the photocurrent response averaged over the last 30 min of the 1st, 2nd, 3rd, 4th, and 5th light cycles for untreated *Synechocystis* cells (Syn(wt), green), PDA-coated cells (Syn-PDA, gray), *Synechocystis* cells physically mixed with abiotically formed PDA (PDA + Syn(wt), orange), and abiotic PDA samples (PDA, blue). Error bars represent one standard deviation from the calculated mean for 6 replicates of the PDA-coated cells and 3 replicates for the other samples (the individual curves in mediated conditions are shown in Fig. S5(B)). Inset: Mean CA photocurrent at the corresponding time intervals. Samples were cyclically exposed to dark and light conditions. The current density was obtained by dividing current values with the geometrical area of the graphite rod (~ 0.7 cm^2). The shaded region represents one standard deviation from the mean. (c) SEM micrographs of graphite foil electrodes with unmodified (left, green frame) and PDA-modified (right, black frame) *Synechocystis* cells at two different magnifications. Additional images can be found in Fig. S7 in the ESM.

which no longer showed a decaying DA oxidation peak (Fig. 4(a)).

After stabilization, the exoelectrogenicity of the cells was characterized under a constant potential of 0.3 V (vs. Ag/AgCl) in the presence of 1 mM $K_3Fe(CN)_6$, which serves as a mediator to transfer charge from the cells to the electrode. Under these mediated conditions, the PDA-coated *Synechocystis* electrode shows a three-fold increase in photocurrent compared to both the unmodified *Synechocystis* and abiotic PDA controls (Fig. 4(b) and Fig. S5(b) in the ESM). The PDA-coated cells further show a higher photocurrent compared to control measurements of abiotically pre-formed PDA mixed with unmodified *Synechocystis* cells. Whereas the mixed sample shows an additive effect of the PDA and *Synechocystis* cells, under mediated conditions, the PDA-coated cells show an enhancement that is synergistic. The *in vivo* polymerization of the PDA-coated cells was thus found to have a beneficial effect on the photocurrent.

The mechanism of this enhancement was studied through SEM imaging and temperature-dependent CA analysis. SEM imaging was used to examine possible differences in cell adhesion in the presence and absence of the PDA coating (Fig. 4(c) and Fig. S7 in the ESM). The SEM images show a significant increase in the electrode coverage of the coated cells compared to the uncoated ones. These observations are consistent with previous reports that have attributed light-responsive polymer enhancements to increased cell adherence [21, 23]. The extent of possible photothermal effects, which have been previously observed for PDA [55, 56], was also studied using temperature-dependent CA measurements. As shown in Fig. S8(a) in the ESM, both the unmodified and the PDA-modified cells show slightly higher baseline activities under light and dark conditions when incubated at an elevated temperature of 30 °C compared to room temperature (ca. 21 °C). These findings may reflect the higher metabolic activity of *Synechocystis* cells when grown at an ideal growth temperature of 30 °C [57, 58]. Accounting for this baseline activity, however, both the unmodified and PDA-modified cells show comparable light-dark responses at room temperature and at 30 °C (Fig. S8(b) in the ESM). The thermal effects therefore do not result in any photo-specific enhancement of the cell response. Although the PDA could enhance the photocurrent through the photothermal increase of the metabolism when under illumination, the illumination measurements do not show any time delay that is otherwise reported for cells adapting their

metabolisms to higher temperatures [59]. In addition, the magnitude of the PDA photocurrent enhancement significantly exceeds the enhancement that is observed on heating the cells to their optimal metabolic temperature. These observations indicate a negligible contribution of the PDA photothermal effects in enhancing the photocurrent.

4 Conclusion

This study identifies the PDA encapsulation conditions for sustaining the growth and enhancing the exoelectrogenicity of *Synechocystis* cells under mediated conditions. The PDA encapsulation is achieved through *in situ* oxygenic polymerization of DA under slightly alkaline environments. The packing of the PDA nanoparticles on the cell surface is found to vary with both the pH of the synthesis solution as well as the initial concentration of DA. Although the oxygen evolution rate of the cells is shown to decrease with increasing PDA formation, cell growth can be sustained at moderate DA concentrations (1 mM) and low pH (pH 7.5) conditions with low PDA surface coverage. Under the tested conditions, the treated cells show a three-fold enhancement in photocurrent under mediated conditions compared to cells in the absence of PDA coating and to PDA in the absence of living cells.

The mechanism of this enhancement is attributed to improved cell adhesion and enhanced conductivity across the cell surface, as reported in previous studies [43]. In contrast to the cells used in these previous studies, however, the *Synechocystis* cells show competitive light absorption within the same range as PDA absorption. While the study herein has focused on mitigating these effects by tuning PDA surface coverage with different pH and monomer concentrations, alternative strategies include using bioengineered or natural light-harvesting microbes with absorption peaks that are distinct from those of the PDA. Such strategies may enable higher concentrations of PDA to further enhance cell exoelectrogenicity without compromising viability. Nonetheless, the demonstration herein establishes previously unexplored metrics for applying a state-of-the-art biosynthetic conductive polymer to photoautotrophs. The sustained growth and the enhanced exoelectrogenicity found under the tested conditions open a window of opportunity for engineering next generation living photovoltaics based on biosynthesized electrodes.

Acknowledgements

The authors are thankful for support from the Swiss National Science Foundation (Sinergia Project, No. IZLIZ2_182972).

Electronic Supplementary Material: Supplementary material (TEM and SEM micrographs of PDA-coated cells obtained using 15 mM DA, SEM images of abiotic PDA particles, Raman spectra of Syn-PDA samples, additional confocal images, CVs of biophotoanodes and abiotic samples, photocurrents responses (CAs) of biotic and abiotic samples in unmediated conditions, SEM images of biotic electrodes, CAs of biotic electrodes at higher temperature) is available in the online version of this article https://doi.org/10.1007/s12274-023-6396-1.

Funding note: Open access publishing supported by EPFL Lausanne.

References

[1] McCormick, A. J.; Bombelli, P.; Bradley, R. W.; Thorne, R.; Wenzel, T.; Howe, C. J. Biophotovoltaics: Oxygenic photosynthetic organisms in the world of bioelectrochemical systems. *Energy Environ. Sci.* **2015**, *8*, 1092–1109.

[2] Mouhib, M.; Antonucci, A.; Reggente, M.; Amirjani, A.; Gillen, A. J.; Boghossian, A. A. Enhancing bioelectricity generation in microbial fuel cells and biophotovoltaics using nanomaterials. *Nano Res.* **2019**, *12*, 2184–2199.

[3] Schuergers, N.; Werlang, C.; Ajo-Franklin, C. M.; Boghossian, A. A. A synthetic biology approach to engineering living photovoltaics. *Energy Environ. Sci.* **2017**, *10*, 1102–1115.

[4] Tschörtner, J.; Lai, B.; Krömer, J. O. Biophotovoltaics: Green power generation from sunlight and water. *Front. Microbiol.* **2019**, *10*, 866.

[5] Wey, L. T.; Bombelli, P.; Chen, X. L.; Lawrence, J. M.; Rabideau, C. M.; Rowden, S. J.; Zhang, Z.; Howe, C. J. The development of biophotovoltaic systems for power generation and biological analysis. *ChemElectroChem* **2019**, *6*, 5375–5386.

[6] Lea-Smith, D. J.; Bombelli, P.; Vasudevan, R.; Howe, C. J. Photosynthetic, respiratory and extracellular electron transport pathways in cyanobacteria. *Biochim. Biophys. Acta* **2016**, *1857*, 247–255.

[7] Tanaka, K.; Kashiwagi, N.; Ogawa, T. Effects of light on the electrical output of bioelectrochemical fuel‐cells containing *Anabaena variabilis* M‐2: Mechanism of the post‐illumination burst. *J. Chem. Technol. Biotechnol.* **1988**, *42*, 235–240.

[8] Pisciotta, J. M.; Zou, Y. J.; Baskakov, I. V. Light-dependent electrogenic activity of cyanobacteria. *PLoS One* **2010**, *5*, e10821.

[9] Pisciotta, J. M.; Zou, Y. J.; Baskakov, I. V. Role of the photosynthetic electron transfer chain in electrogenic activity of cyanobacteria. *Appl. Microbiol. Biotechnol.* **2011**, *91*, 377–385.

[10] Saper, G.; Kallmann, D.; Conzuelo, F.; Zhao, F. Y.; Tóth, T. N.; Liveanu, V.; Meir, S.; Szymanski, J.; Aharoni, A.; Schuhmann, W. et al.. Live cyanobacteria produce photocurrent and hydrogen using both the respiratory and photosynthetic systems. *Nat. Commun.* **2018**, *9*, 2168.

[11] Mouhib, M.; Reggente, M.; Li, L.; Schuergers, N.; Boghossian, A. A. Tailored extracellular electron transfer pathways enhance the electroactivity of Escherichia coli. *bioRxiv* **2021**.

[12] Longatte, G.; Rappaport, F.; Wollman, F. A.; Guille-Collignon, M.; Lemaître, F. Electrochemical harvesting of photosynthetic electrons from unicellular algae population at the preparative scale by using 2, 6-dichlorobenzoquinone. *Electrochim. Acta* **2017**, *236*, 337–342.

[13] Bombelli, P.; Zarrouati, M.; Thorne, R. J.; Schneider, K.; Rowden, S. J. L.; Ali, A.; Yunus, K.; Cameron, P. J.; Fisher, A. C.; Ian Wilson, D.; et al. Surface morphology and surface energy of anode materials influence power outputs in a multi-channel mediatorless bio-photovoltaic (BPV) system. *Phys. Chem. Chem. Phys.* **2012**, *14*, 12221–12229.

[14] Liu, L.; Choi, S. Self-sustainable, high-power-density bio-solar cells for lab-on-a-chip applications. *Lab Chip* **2017**, *17*, 3817–3825.

[15] Wenzel, T.; Härtter, D.; Bombelli, P.; Howe, C. J.; Steiner, U. Porous translucent electrodes enhance current generation from photosynthetic biofilms. *Nat. Commun.* **2018**, *9*, 1299.

[16] Hasan, K.; Yildiz, H. B.; Sperling, E.; Conghaile, P. Ó.; Packer, M. A.; Leech, D.; Hägerhäll, C.; Gorton, L. Photo-electrochemical communication between cyanobacteria (*Leptolyngbia* sp) and

osmium redox polymer modified electrodes. *Phys. Chem. Chem. Phys.* **2014**, *16*, 24676–24680.
[17] Hasan, K.; Çevik, E.; Sperling, E.; Packer, M. A.; Leech, D.; Gorton, L. Photoelectrochemical wiring of *Paulschulzia pseudovolvox* (algae) to osmium polymer modified electrodes for harnessing solar energy. *Adv. Energy Mater.* **2015**, *5*, 1501100.
[18] Hasan, K.; Grippo, V.; Sperling, E.; Packer, M. A.; Leech, D.; Gorton, L. Evaluation of photocurrent generation from different photosynthetic organisms. *ChemElectroChem* **2017**, *4*, 412–417.
[19] Sekar, N.; Umasankar, Y.; Ramasamy, R. P. Photocurrent generation by immobilized cyanobacteria via direct electron transport in photo-bioelectrochemical cells. *Phys. Chem. Chem. Phys.* **2014**, *16*, 7862–7871.
[20] Zou, Y. J.; Pisciotta, J.; Billmyre, R. B.; Baskakov, I. V. Photosynthetic microbial fuel cells with positive light response. *Biotechnol. Bioeng.* **2009**, *104*, 939–946.
[21] Reggente, M.; Politi, S.; Antonucci, A.; Tamburri, E.; Boghossian, A. A. Design of optimized PEDOT‐based electrodes for enhancing performance of living photovoltaics based on phototropic bacteria. *Adv. Mater. Technol.* **2020**, *5*, 1900931.
[22] Chen, X. L.; Lawrence, J. M.; Wey, L. T.; Schertel, L.; Jing, Q. S.; Vignolini, S.; Howe, C. J.; Kar-Narayan, S.; Zhang, J. Z. 3D-printed hierarchical pillar array electrodes for high-performance semi-artificial photosynthesis. *Nat. Mater.* **2022**, *21*, 811–818.
[23] Roullier, C.; Reggente, M.; Gilibert, P.; Boghossian, A. A. Polypyrrole electrodes show strain‐specific enhancement of photocurrent from cyanobacteria. *Adv. Mater. Technol.* **2023**, *8*, 2201839.
[24] Clifford, E. R.; Bradley, R. W.; Wey, L. T.; Lawrence, J. M.; Chen, X. L.; Howe, C. J.; Zhang, J. Z. Phenazines as model low-midpoint potential electron shuttles for photosynthetic bioelectrochemical systems. *Chem. Sci.* **2021**, *12*, 3328–3338.
[25] Sekar, N.; Jain, R.; Yan, Y. J.; Ramasamy, R. P. Enhanced photo‐bioelectrochemical energy conversion by genetically engineered cyanobacteria. *Biotechnol. Bioeng.* **2016**, *113*, 675–679.
[26] Reggente, M.; Schurgers, N.; Mouhib, M.; Politi, S.; Antonucci, A.; Boghossian, A. A. Living photovoltaics based on recombinant expression of MtrA decaheme in photosynthetic bacteria. *bioRxiv* 2023.
[27] Meng, H. K.; Zhang, W.; Zhu, H. W.; Yang, F.; Zhang, Y. P.; Zhou, J.; Li, Y. Over-expression of an electron transport protein OmcS provides sufficient NADH for D-lactate production in cyanobacterium. *Biotechnol. Biofuels* **2021**, *14*, 109.
[28] Antonucci, A.; Reggente, M.; Roullier, C.; Gillen, A. J.; Schuergers, N.; Zubkovs, V.; Lambert, B. P.; Mouhib, M.; Carata, E.; Dini, L. et al. Carbon nanotube uptake in cyanobacteria for near-infrared imaging and enhanced bioelectricity generation in living photovoltaics. *Nat. Nanotechnol.* **2022**, *17*, 1111–1119.
[29] Liu, L.; Choi, S. Enhanced biophotoelectricity generation in cyanobacterial biophotovoltaics with intracellularly biosynthesized gold nanoparticles. *J. Power Sources* **2021**, *506*, 230251.
[30] Wang, S.; Guo, Z. G. Bio-inspired encapsulation and functionalization of living cells with artificial shells. *Colloids Surf. B Biointerfaces* **2014**, *113*, 483–500.
[31] Yang, S. H.; Lee, K. B.; Kong, B.; Kim, J. H.; Kim, H. S.; Choi, I. S. Biomimetic encapsulation of individual cells with silica. *Angew. Chem., Int. Ed.* **2009**, *48*, 9160–9163.
[32] Fakhrullin, R. F.; Minullina, R. T. Hybrid cellular-inorganic core-shell microparticles: Encapsulation of individual living cells in calcium carbonate microshells. *Langmuir* **2009**, *25*, 6617–6621.
[33] Yang, S. H.; Ko, E. H.; Choi, I. S. Cytocompatible encapsulation of individual *Chlorella* cells within titanium dioxide shells by a designed catalytic peptide. *Langmuir* **2012**, *28*, 2151–2155.
[34] Apetrei, R. M.; Carac, G.; Bahrim, G.; Ramanaviciene, A.; Ramanavicius, A. Modification of *Aspergillus niger* by conducting polymer, Polypyrrole, and the evaluation of electrochemical properties of modified cells. *Bioelectrochemistry* **2018**, *121*, 46–55.
[35] Song, R. B.; Wu, Y. C.; Lin, Z. Q.; Xie, J.; Tan, C. H.; Loo, J. S. C.; Cao, B.; Zhang, J. R.; Zhu, J. J.; Zhang, Q. C. Living and conducting: Coating individual bacterial cells with *in situ* formed polypyrrole. *Angew. Chem.* **2017**, *129*, 10652–10656.
[36] Labarile, R.; Varsalona, M.; Vona, D.; Stufano, P.; Grattieri, M.; Farinola, G. M.; Trotta, M. A novel route for anoxygenic polymerization of dopamine via purple photosynthetic bacteria metabolism. *MRS Adv.* **2023**, *8*, 423–428.
[37] Liu, Y. L.; Ai, K. L.; Lu, L. H. Polydopamine and its derivative materials: Synthesis and promising applications in energy, environmental, and biomedical fields. *Chem. Rev.* **2014**, *114*, 5057–5115.
[38] Kim, J. H.; Lee, M.; Park, C. B. Polydopamine as a biomimetic electron gate for artificial photosynthesis. *Angew. Chem.* **2014**, *126*, 6482–6486.
[39] Du, Q.; Li, T.; Li, N.; Wang, X. Protection of electroactive biofilm from extreme acid shock by polydopamine encapsulation. *Environ. Sci. Technol. Lett.* **2017**, *4*, 345–349.
[40] Yang, S. H.; Kang, S. M.; Lee, K. B.; Chung, T. D.; Lee, H.; Choi, I. S. Mussel-inspired encapsulation and functionalization of individual yeast cells. *J. Am. Chem. Soc.* **2011**, *133*, 2795–2797.
[41] Dreyer, D. R.; Miller, D. J.; Freeman, B. D.; Paul, D. R.; Bielawski, C. W. Perspectives on poly(dopamine). *Chem. Sci.* **2013**, *4*, 3796–3802.
[42] Wang, L.; Hu, Z. Y.; Yang, X. Y.; Zhang, B. B.; Geng, W.; van Tendeloo, G.; Su, B. L. Polydopamine nanocoated whole-cell asymmetric biocatalysts. *Chem. Commun.* **2017**, *53*, 6617–6620.
[43] Liu, S. R.; Cai, L. F.; Wang, L. Y.; Yi, X. F.; Peng, Y. J.; He, N.; Xue, X. E.; Wang, Y. P. Polydopamine coating on individual cells for enhanced extracellular electron transfer. *Chem. Commun.* **2019**, *55*, 10535–10538.
[44] Buscemi, G.; Vona, D.; Stufano, P.; Labarile, R.; Cosma, P.; Agostiano, A.; Trotta, M.; Farinola, G. M.; Grattieri, M. Bio-inspired redox-adhesive polydopamine matrix for intact bacteria biohybrid photoanodes. *ACS Appl. Mater. Interfaces* **2022**, *14*, 26631–26641.
[45] Rippka, R.; Deruelles, J.; Waterbury, J. B.; Herdman, M.; Stanier, R. Y. Generic assignments, strain histories and properties of pure cultures of cyanobacteria. *J. Gen. Microbiol.* **1979**, *111*, 1–61.
[46] Ritchie, R. J. Consistent sets of spectrophotometric chlorophyll equations for acetone, methanol and ethanol solvents. *Photosyn. Res.* **2006**, *89*, 27–41.
[47] Zubkovs, V.; Antonucci, A.; Schuergers, N.; Lambert, B.; Latini, A.; Ceccarelli, R.; Santinelli, A.; Rogov, A.; Ciepielewski, D.; Boghossian, A. A. Spinning-disc confocal microscopy in the second near-infrared window (NIR-II). *Sci. Rep.* **2018**, *8*, 13770.
[48] Hyun Ryu, J.; Messersmith, P. B.; Lee, H. Polydopamine surface chemistry: A decade of discovery. *ACS Appl. Mater. Interfaces* **2018**, *10*, 7523–7540.
[49] Wei, Q.; Zhang, F. L.; Li, J.; Li, B. J.; Zhao, C. S. Oxidant-induced dopaminepolymerization for multifunctional coatings. *Polym. Chem.* **2010**, *1*, 1430–1433.
[50] Jehlička, J.; Edwards, H. G. M.; Osterrothová, K.; Novotná, J.; Nedbalová, L.; Kopecký, J.; Němec, I.; Oren, A. Potential and limits of Raman spectroscopy for carotenoid detection in microorganisms: Implications for astrobiology. *Philos. Trans. Roy. Soc. A Math. Phys. Eng. Sci.* **2014**, *372*, 20140199.
[51] Alfieri, M. L.; Panzella, L.; Oscurato, S. L.; Salvatore, M.; Avolio, R., Errico, M. E.; Maddalena, P.; Napolitano, A.; D'Ischia, M. The chemistry of polydopamine film formation: The amine-quinone interplay. *Biomimetics* **2018**, *3*, 26.
[52] Scheer, H. *Chlorophylls*; CRC Press: Boca Raton, 1991.
[53] Schulze, K.; López, D. A.; Tillich, U. M.; Frohme, M. A simple viability analysis for unicellular cyanobacteria using a new autofluorescence assay, automated microscopy, and ImageJ. *BMC Biotechnol.* **2011**, *11*, 118.
[54] Ponzio, F.; Ball, V. Persistence of dopamine and small oxidation products thereof in oxygenated dopamine solutions and in "polydopamine" films. *Colloids Surf. A Physicochem. Eng. Aspects* **2014**, *443*, 540–543.
[55] Bu, T.; Tian, Y. M.; Ma, J.; Zhang, M.; Bai, F. E.; Zhao, S.; He, K. Y.; Sun, X. Y.; Wang, Y.; Wang, L. Polydopamine-mediated photothermal effect enables a new method for point-of-care testing of biothiols using a portable photothermal sensor. *Sens. Actuators B Chem.* **2021**, *346*, 130498.
[56] Fan, S. B.; Lin, W. S.; Huang, Y. F.; Xia, J. J.; Xu, J. F.; Zhang, J.

H.; Pi, J. Advances and potentials of polydopamine nanosystem in photothermal-based antibacterial infection therapies. *Front. Pharmacol.* **2022**, *13*, 829712.

[57] Tasaka, Y.; Gombos, Z.; Nishiyama, Y.; Mohanty, P.; Ohba, T.; Ohki, K.; Murata, N. Targeted mutagenesis of acyl‐lipid desaturases in Synechocystis: Evidence for the important roles of polyunsaturated membrane lipids in growth, respiration and photosynthesis. *EMBO J.* **1996**, *15*, 6416–6425.

[58] Hasunuma, T.; Matsuda, M.; Kato, Y.; Vavricka, C. J.; Kondo, A. Temperature enhanced succinate production concurrent with increased central metabolism turnover in the cyanobacterium *Synechocystis* sp. PCC 6803. *Metab. Eng.* **2018**, *48*, 109–120.

[59] Červený, J.; Sinetova, M. A.; Zavřel, T.; Los, D. A. Mechanisms of high temperature resistance of *Synechocystis* sp. PCC 6803: An impact of histidine kinase 34. *Life* **2015**, *5*, 676–699.